An ultra-low magnetic field thermal demagnetizer for high-precision paleomagnetism

Huafeng Qin (huafeng_qin@mail.iggcas.ac.cn)
Institute of Geology and Geophysics Chinese Academy of Sciences https://orcid.org/0000-0001-7699-5161

Xiang Zhao
Australian National University

Shuangchi Liu
Institute of Geology and Geophysics Chinese Academy of Sciences

Greig Paterson
University of Liverpool

Zhaoxia Jiang
Ocean University of China

Shuhui Cai
Institute of Geology and Geophysics Chinese Academy of Sciences

Jinhua Li
Institute of Geology and Geophysics Chinese Academy of Sciences

Qingsong Liu
Southern University of Science and Technology

Rixiang Zhu
Institute of Geology and Geophysics Chinese Academy of Sciences

Technical report

Keywords: Paleomagnetism, thermal demagnetization, furnace, AC magnetic field, residual magnetic field□heating wire structure, straight core solenoid

Posted Date: November 2nd, 2020

DOI: https://doi.org/10.21203/rs.3.rs-54689/v3

Version of Record: A version of this preprint was published on November 4th, 2020. See the published version at https://doi.org/10.1186/s40623-020-01304-0.

An ultra-low magnetic field thermal demagnetizer for high-precision paleomagnetism

Huafeng Qin[1*], Xiang Zhao[1,2], Shuangchi Liu[1], Greig A. Paterson[3,4], Zhaoxia Jiang[1,5], Shuhui Cai[1], Jinhua Li[3], Qingsong Liu[1,6], Rixiang Zhu[1]

*Correspondence: huafeng_qin@mail.iggcas.ac.cn

[1] State Key Laboratory of Lithospheric Evolution, Institute of Geology and Geophysics, Chinese Academy of Sciences, Beijing 100029, China

Full list of author information is available at the end of the article

Abstract

Thermal demagnetization furnaces are widely used paleomagnetic facilities for progressive removal of naturally acquired magnetic remanence or the imparting of well controlled laboratory magnetization. An ideal thermal demagnetizer should maintain “zero” magnetic field in the sample chamber during thermal treatments. However, magnetic field noises, including the residual magnetic fields of the construction material and the induced fields caused by the alternating current (AC) in the heating element are always present, which can contaminate the paleoamgnetic results at the elevated temperatures or especially for the magnetically weak samples. Here, we designed a new structure of heating wire named “straight core solenoid” to develop a new demagnetization furnace with ultra-low magnetic field noise. Simulation and practical measurements show that the heating current magnetic field can be greatly reduced by using the new technology. Thermal demagnetization experiments demonstrate that the new demagnetizer can yield low noise results even for weakly magnetic samples.

Key words:

Paleomagnetism, thermal demagnetization, furnace, AC magnetic field, residual magnetic field，heating wire structure, straight core solenoid

1. Introduction

Paleomagnetism investigates changes in the geomagnetic field through geologic time by the measurement of natural remanent magnetizations (NRM) recorded by magnetic minerals in natural materials. NRM of geological materials usually consists of multiple components. Therefore, to define the stable characteristic remanent magnetization (ChRM) of geological interests, the secondary remanent magnetization needs be removed using sequential demagnetization techniques (e.g., the step-wise progressive thermal or alternating field demagnetization) (Irving et al., 1961; Schmidt, 1993). During thermal demagnetization, specimens are heated to a pre-selected temperature, held for a period of time (e.g., 10-30 minutes), and then cooled down to the room temperature in "zero" magnetic field environment (Collinson, 1983). This treatment will be conducted repeatedly in a stepwise manner till the ChRM is isolated (Thellier, 1966; Collinson, 1975). Thermal demagnetization is one of the standard demagnetization methods, and thus thermal demagnetization furnaces (or thermal demagnetizers) have been widely equipped in nearly all paleomagnetic laboratories.

Although widely used, the experimental success rate of thermal demagnetization can be relatively low especially for weakly magnetic samples such as sedimentary rocks. It is often found

that remanent direction of some specimens become seriously distorted at high temperatures, but the ChRM can still be obtained by alternating field demagnetization using sister specimens (e.g., Holm and Verosub, 1988). The failure of thermal demagnetization could be attributed to irreversible thermal physio-chemical alterations upon heating (e.g., Wasilewski 1969, Heller et al., 1970), partial thermoremanent magnetization (pTRM) acquisition in the presence of a residual DC field upon cooling (Collinson, 1975), or magnetic fields caused by the heating current (Heller et al., 1970). Although early studies did not detect differences between inductive and noninductive heating wire (Irving et al., 1961), inductive alternating fields (AF) can cause unwanted AF demagnetization behavior at high temperatures. Given that the coercivity of magnetic minerals reduces quickly as the temperature approaches the unblocking temperature or Curie temperature, this effect may be substantial. In the extreme, the NRM direction could be biased by single axis AF demagnetization because of the stationary current field (Stephenson, 1983) at high temperature.

Reducing the residual fields in thermal demagnetizers can significantly improve the quality of paleomagnetic measurements, particularly for weakly magnetized specimens. Moreover, for the study of meteorites in planetary science or magnetizations acquired near the onset of the geodynamo, understanding the characteristic remanent magnetization acquired in low magnetic fields, including extremely weak fields (nT range) is a topic of great interest (Weiss et al., 2010; Tarduno et al., 2015; Wang et al., 2017). It is important that the technology around thermal demagnetizers progress to keep pace with the changing demands of the scientific community.

In this study, we will first describe the technology to reduce the residual magnetic field for a newly designed thermal demagnetizer. The key point is to reduce the current magnetic field by adopting a new structure of heating element. We then conduct thermal demagnetization experiments

to test the performance of the new furnace.

2. Newly designed furnace for thermal demagnetization

The heating elements in thermal demagnetizers is typically constructed of non-inductive windings in order to minimize the AC demagnetization effect of the heating current (Chamalaun, 1964). There are generally two types of non-inductive heater winding, one is a bifilar solenoid wrapped on a cylindrical form to heat specimens within (Figure 1a). This style of winding is widely used in small furnaces such as the Sogo Fine-TD furnace in Japan (Zheng et al., 2010). It is also used in some Kappabridges and variable field translation balances (VFTBs) to heat specimens. In this configuration, the opposing currents of adjacent wires reduce the AC magnetic field. In addition, the wire spacing should be small enough to efficiently reduce the residual magnetic field. A disadvantage of this system, however, is that it will increase the risk of short circuit, and often lead to limited sample capacity in order to maintain an acceptable resistance and workable power consumption.

An alternative method is to use solenoids arranged in opposite direction (Figure 1b) or wound into a helix as in many commercial furnaces. It is usually assumed that the magnetic field generated by a uniform solenoid is only in the interior and both ends of the solenoid, but this neglects the fact that for a real solenoid the wire loops (and current loops) are not perfectly circular, the current must go from one end to the other, which results in non-zero external fields. Therefore, it is necessary to consider the magnetic field distribution outside a helical solenoid.

2.1. Simulated calculation of solenoid magnetic field

The magnetic field distribution outside a solenoid can be calculated using the Biot-Savart law

(Hagel et al., 1994; Budnik and Machczynski, 2011). Assuming a current, *I*, flowing in a finite solenoid with a radius of *R* and and a pitch of *p*, the vectors of magnetic field at point P (Figure 2) produce by a differential current element *Idl* at source point N(*Xs*, *Ys*, *Zs*) can be written as:

$$dB = \frac{\mu_0 I}{4\pi}\frac{d\vec{l}\times\vec{r}}{r^3}, \tag{1}$$

where *r* is distance from the point N on the filament to the field point P. $Xs=R\cos\Theta$, $Ys=R\sin\Theta$ and $Zs=a\Theta$ since the point N is on the solenoid, where *a* is the pitch factor.

From cylindrical coordinates to Cartesian coordinates, *dl* and *r* can be expressed as:

$$d\vec{l} = \vec{i}\,dx + \vec{j}dy + \vec{k}dz = -\vec{i}R\sin\theta d\theta + \vec{j}R\cos\theta d\theta + \vec{k}ad\theta \tag{2}$$

$$\vec{r} = \vec{i}\,(x_0 - R\cos\theta) + \vec{j}(y_0 - R\sin\theta) + \vec{k}(z_0 - a\theta). \tag{3}$$

Therefore:

$$d\vec{l}\times\vec{r} = \begin{vmatrix} \vec{i} & \vec{j} & \vec{k} \\ -R\sin\theta d\theta & R\cos\theta d\theta & ad\theta \\ x_0 - R\cos\theta & y_0 - R\sin\theta & z_0 - a\theta \end{vmatrix}, \tag{4}$$

and we have

$$dB_x = \frac{\mu_0 I}{4\pi}\frac{\left[(z_0 - a\theta)R\cos\theta - (y_0 - R\sin\theta)a\right]d\theta}{\left[(x_0 - R\cos\theta)^2 + (y_0 - R\sin\theta)^2 + (z_0 - a\theta)^2\right]^{3/2}} \tag{5}$$

$$dB_y = \frac{\mu_0 I}{4\pi}\frac{\left[(z_0 - a\theta)R\sin\theta + (x_0 - R\cos\theta)a\right]d\theta}{\left[(x_0 - R\cos\theta)^2 + (y_0 - R\sin\theta)^2 + (z_0 - a\theta)^2\right]^{3/2}} \tag{6}$$

$$dB_z = -\frac{\mu_0 I}{4\pi}\frac{\left[(y_0 - R\sin\theta)R\sin\theta + (x_0 - R\cos\theta)R\cos\theta\right]d\theta}{\left[(x_0 - R\cos\theta)^2 + (y_0 - R\sin\theta)^2 + (z_0 - a\theta)^2\right]^{3/2}}. \tag{7}$$

As the radius of the solenoid decreases, or when the distance between the point P and solenoid is much larger than the radius, R can be approximately ignored. The point N on a straight wire is $(0,0,a\theta)$, and filament became as $d\vec{l} = \vec{k}ad\theta$, and $\vec{r} = \vec{i}x_0 + \vec{j}y_0 + \vec{k}(z_0 - a\theta)$, and therefore, the formula of magnetic field can be simplified as:

$$dB_x = -\frac{\mu_0 I}{4\pi} \frac{y_0 a d\theta}{\left[x_0^{\,2} + y_0^{\,2} + (z_0 - a\theta)^2\right]^{3/2}} \tag{9}$$

$$dB_y = \frac{\mu_0 I}{4\pi} \frac{x_0 a d\theta}{\left[x_0^{\,2} + y_0^{\,2} + (z_0 - a\theta)^2\right]^{3/2}} \tag{10}$$

$$dB_z = 0 \tag{11}$$

It can be seen that when the solenoid diameter is small, the magnetic field generated by the solenoid is roughly the same as that of a straight wire. Therefore, to reduce the stray external fields of a solenoid, a straight wire can be inserted through its core and connected with solenoid at one end, such that the current in the straight wire is flowing opposite to the current in the solenoid (Figure 1c). A new heating element is designed based on this configuration which we call it straight core solenoid, and will be used to manufacture our new thermal demagnetizer.

To simulate a heating element solenoid, we assume that the solenoid length is 1 m, the radius is 4 mm, and the pitch is also 4 mm. And the current is set to 1A. We simulate the fields in YZ plane (Figure 2) along the direction of solenoid axis, at a distance of 20 mm and 10 mm from central axis. The results are shown in Figure 3. Only absolute values of field are shown in Figure 3a because of the logarithmic scale. It is found that the perpendicular component (X) is higher than the radial component (Y) and parallel components (Z), and the X component can be reduced by two orders of magnitude if a straight wire with reverse current is passed through the center of the solenoid. The Y and Z components remain unchanged, since the magnetic field produced by the straight wire wraps around the wire, which is shown here in the X direction only. The fluctuations of field value were also observed at very close to the solenoid and the period is consistent with the pitch (Figure 3b). As the distance increases, the periodic fluctuation becomes insignificant (Hagel et al., 1994). The magnetic field distribution in other cases can be obtained by changing parameters of the solenoid, such as radius, pitch. It is useful to optimize the structure of heating wire before practical manufacture.

In fact, the whole heater group consists of a series of parallel or anti-parallel heating element

solenoid and its configuration determined the magnetic field inside the furnace. We calculate the magnetic field distribution in the furnace. The heater composed of 12 conventional solenoids or new heating elements with opposite current direction between adjacent is simulated. Contour maps of different components are shown in Figure 4. The parameters of each solenoid are the same as those used in Figure 3, and the current is still set to 1A. X, Y and Z represent the magnetic field in horizontal, vertical and along the axis direction in the furnace, respectively. It can be seen that the magnetic field in the center of the furnace is extremely low for both configurations, but the low magnetic field area is considerably enlarged in the furnace with new heating elements. The magnetic field inside the solenoid is relatively complex, but does not affect the thermal demagnetization samples. Different configurations which are consistent with some practical applications can also be simulated. A large magnetic field may be produced by parallel connection of heating wire groups (Figure 5). However, the magnetic field is still very low inside the furnace with same configuration using the new straight core solenoid.

2.2. Measurement of solenoid magnetic field

In order to verify the effectiveness and determine the magnetic field of the new heating element, the respective magnetic fields produce by the conventional solenoid heating wire and the new heating element were measured with a triaxial fluxgate magnetometer (APS520). One solenoid heating element with length of one meter and diameter of 8 mm was placed inside a magnetically shielding cylinder with 1A DC current applied in the wire (Figure 6a). The fluxgate sensor was placed to the side of solenoid at vertical distance of about 20 mm and moved along the long axis direction. The magnetic field at different positions was observed with the current on then off. In the same way, we measured the magnetic field of our new straight core solenoid heating element, which is composed of the same solenoid with a straight wire passing through it (Figure 6b). The solenoid and the straight wire were isolated by a ceramic sheath. The results are shown in Figure 6c. The magnetic field of conventional solenoid is about 6000–7000 nT and field direction is almost perpendicular to the long axis of solenoid and is consistent with the simulation, which is almost

equivalent to that of an axial line current. The stray magnetic field of the straight core solenoid is much lower than the standard solenoid, with a total field intensity of 26-535 nT.

In our prototype thermal demagnetizer adjacent elements are arranged in opposite directions (Figure 7a). The magnetic field at different positions along the axis of the heating chamber were measured when a DC current of 1A is applied to the heating wire. We measured the magnetic field four times at different vertical distances from the center axis. The peak magnetic field in the sample region is about 130 nT (Figure 7b). In order to verify the effect, we also arranged the conventional solenoids following the same structure, and the current of adjacent solenoids is opposite. It is found that the magnetic field in the center is relatively low (115-285 nT in sample zone), but gradually increases toward the edge of the furnace (Figure 7c). However, if the wire connection are changed, parallel connection of two groups are adopted, the magnetic field will become higher and mainly in the vertical direction (Figure 7d). The measured results are consistent with the numerical simulation.

2.3 Degaussing the shield cylinder and the TD-PGL-100

In order to shield the influence of external magnetic field, the chamber of thermal demagnetization furnace is usually installed in a cylindrical magnetic shield cylinder. The residual fields in sample zone typically vary from several nT to 150 nT in different furnaces (Paterson et al., 2012), which is mainly determined by the remanent magnetization of magnetic materials within the furnace, especially the shields (Freake and Thorp, 1971, Thiel et al., 2007). A lower residual field can be achieved by AF demagnetization of the shield cylinder. Early experiments found that the best shield demagnetization results were obtained by passing the AC current through conductors within the shield cylinders or by passing the current longitudinally through the shielding material

itself (Herrmannsfeldt and Salsburg, 1964). A circular magnetic field perpendicular to the central longitudinal axis will be produced in the cylindrical shield if a current conducting straight wire is passed though the longitudinal center axis of the shield cylinder, however, this requires a large current to reach peak demagnetization. In practice, we use a total of eight 4 mm^2 copper lines wound from inside to outside of the shield cylinder to form a large coil (Figure 8a), and connected to a transformer with a twisted-pair cable. The transformer has separated primary and secondary windings which can be pulled apart. Separating the windings will generate a nonlinear attenuation of the alternating current in the coil which performs AF demagnetization of the shield cylinder. The residual magnetic field in the sample region can be as low as 1 nT (Figure 8b), which makes it possible to further reduce spurious fields during thermal demagnetization.

A new furnace named TD-PGL-100 had been built based on above mentioned techniques. The furnace has a chamber of 120 cm length and 9 cm diameter, and the sample zone is designed as 60 cm in length, which allows up to 100 standard paleomagnetic specimens be treated together. Temperature gradient in the sample zone is within 10°C of target temperature below 600°C and 12°C at 700°C. The maximum power consumption of the furnace is 4.0 KVA. Employing an adjustable voltage silicon-controlled rectifier over a solid-state relay allows the output power to be decreased as the temperature approaches the target point, which helps to avoid temperature overshoots. With careful tuning, the oven temperature has a 1°C accuracy with a resolution of 0.1°C. As the examples of heating and cooling curves shown in the Figure 9, the temperature rises rapidly at the beginning of heating, and gradually approaches the target temperature after ~30 minutes and then the temperature is maintained for a hold time to ensure the samples are thoroughly heated. The

cooling fan can be turned on manually or automatically to cool the samples down. The temperature drops rapidly and slows when approaching room temperature. The heating and cooling data can be logged into USB memory automatically, which is essential for the thermal treatment and related experiments particularly for absolute paleointensity studies, where temperature reproducibility is important.

3. Examples of thermal demagnetization experiment

In order to verify the effectiveness of the new furnace, thermal demagnetization experiments were carried out on 12 natural specimens and 8 synthetic specimens using TD-PGL-100. Nine sandstone specimens denoted as "B" were collected from Cenozoic strata in Yunnan, and three muddy limestone specimens denoted as "CM" were from Tibet. The main magnetic carrier mineral of sandstone specimen is hematite (Li et al., 2017). They have only a single univectorial component decaying steadily toward high temperature. The muddy limestone specimens also contain hematite and have multi-component characteristics of different temperature ranges. Hematite specimens synthesized in the lab were chosen to avoid potential thermochemical changes during multiple heatings. The particles of hematite are cubic (Ozaki et al., 1986; Sugimoto et al., 1993) and with a broadly uniform size distribution with an average length and width of 570 nm and 545 nm, respectively.

We have also tried to evaluate the influence of the background magnetic field. After progressive thermal demagnetization of TRM was carried out to identify the unblocking temperature spectrum of the synthetic hematite specimens, the specimens were heated to 700°C for complete

thermal demagnetization, then the progressive thermal demagnetization was repeated. Remanent directions and moments were measured with a cryogenic magnetometer system (2G Enterprises 755) installed in the magnetically shielded room with residual field < 300 nT at IGGCAS. Background noise is typically lower than $2\times10^{-12}Am^2$, and the background moment of the sample tray was kept less than $5\times10^{-11}Am^2$ during the measurements. All the experiments were completed in the paleomagnetic laboratory at the Institute of Geology and Geophysics, Chinese Academy of Sciences (IGGCAS).

The thermal demagnetization experiments of natural specimens show that good demagnetization results can be obtained using the new furnace. The representative experimental results are shown in Figure 10. The remanence directions of of some specimens do not change much after demagnetization at high temperature, when the remanence intensity is less than 10% of the NRM intensity. The ChRM of high temperature can be successfully isolated for the specimens with multi-component characteristics. The magnetic moments of synthetic specimens during the repeated progressive thermal demagnetization are about 0.02-0.05% of the 30 μT TRM (*see detail in supporting information*). It confirms that the influenced by undesirable magnetic fields from the furnace is very small.

4. Discussion

For comparison, Zheng et al. (2010a) investigated similar 1A current field (~240 nT) for the commercially available Sogo Fine-TD. They also reported 0.5 A current field for the ASC TD48 and Natsuhara as being 3600 and 1600 nT, respectively (equivalent to 1 A fields of 7200 and 3200 nT, respectively). We noticed that they obtained an abnormal field higher than 100 μT at 0.3 A in

the MMTD80 thermal demagnetizer, which may be produced by the applied field coil for the paleointensity experiment. Subsequently, a low field (48.4nT/A along the oven axis and less than 3nT/A at right angles in oven axis) was reported by Shaw (2010), and a relatively higher field of ~840nT/A by Zheng et al (2010b), respectively. Our simulation and experimental results show that the magnetic field inside the furnace using conventional solenoid is non-uniform. Although the heater configuration with conventional solenoids can also cancel out the magnetic field especially at the center, for effective cancellation of the fields generated in each solenoid, this design requires that opposing solenoids are perfectly antiparallel. Imperfect alignment results in small, but potentially significant AC fields when large currents are applied during heating (Zheng et al., 2010a, b; Shaw, 2010). In contrast, the new design with straight core solenoid can reduce the dependence on symmetry of configuration, and can also obtain a large space of low magnetic field.

We use our new straight core solenoid heating element to build a new furnace named TD-PGL-100. Subsequently measurements in our later builds have peak current field of only ~95 nT/A. This new design, which holds up to 100 specimens, represents a 2-3 times reduction in AC fields compared to the eight specimen Sogo Fine-TD, and a 9 to 77 times reductions compared to other high capacity demagnetizers. Yuan et al. (2020) investigated paleomagnetic behavior of red beds in the Sangdanlin section using the new furnace. The results can be reasonably compared with the previously published paleoamgnetic results for the same section using the ASC TD48 by Yang et al. (2019). Clearly, excellent paleomagnetic directional data of high temperature component (650-680℃) can be defined using the data from new furnace, while some remanence directions become erratic after thermal demagnetization at 620-660℃ using the ASC TD48. This comparison supports that the new thermal demagnetizing furnace has better performance.

It should be noted that the current field is an alternating magnetic field. In thermal demagnetization, the current field is more like the effect of AF demagnetization, and the way to cut off the heating current (e.g., abrupt on-off, or gradual ramping etc.) may affect the demagnetization effect. However, the new design combined with the appropriate mode of AC supply has the potential to further lower the impact. Although our improved heating element can greatly reduce the AC current field, it cannot completely eliminate it. If lower AC magnetic fields are required, the only alternative would be to heat the specimens outside of the primary electrical heating element region. This could be achieved by heating the sample region by hot gas flow heated outside the sample region. This style of furnace can reduce AC current field to practically zero (Heller et al., 1970). Such gas flow furnace systems, however, are limited to heating only a small number of specimens. Our new TD-PGL-100 thermal demagnetizer with lower AC current field and super low residual magnetic fields is a reasonable choice for most paleomagnetic laboratories.

5. Conclusions

Here we introduce a new heating element that is composed of a straight wire inserted into solenoid and connected in series at one end, a configuration we call a straight core solenoid. Such a configuration can drastically reduce the stray magnetic fields generated when a current is applied to the heating element. We also adopt a demagnetization procedure that can reduce the residual magnetic field in shield cylinder to less than 1 nT in sample zone. The TD-PGL-100 built with those technologies allows the successful recovery of weak magnetizations blocked at high temperatures and has applications in recovering sedimentary magnetizations, records of geomagnetic polarity reversals, signals of the earliest geodynamo, as well as extraterrestrial magnetizations. One of this new thermal demagnetizer has been running normally for three years in the IGCCAS laboratory,

and results demonstrate its excellent performance especially for these weakly magnetic natural specimens (Jiang et al., 2017, Yan et al., 2018).

6. Acknowledgements

We thank Jie Yuan and Dr Shihu Li for providing the natural samples for testing. We also thank Jeff Gee and three anonymous reviewers for reviewing the earlier version of the manuscript.

List of abbreviations

NRM: The natural remanent magnetization

AC: the alternating current

ChRM: the stable characteristic remanent magnetization

pTRM: partial thermoremanent magnetization

AF: the alternating field

DRM: the detrital remanent magnetization

Authors' contributions

HQ: instrument development; experimental design; figures plotting; manuscript writing. XZ: instrument manufacture;key issues discussion; manuscript revising. SL: test of instrument. GP: key issues discussion; manuscript revising. ZJ: preparation of synthetic samples. SC: Experimental test and data

analysis. JL: key issues discussion. QL: proposing idea; framework design; manuscript revising. RZ: supervision of work and manuscript evaluation. All authors read and approved the final manuscript.

Funding

This work was supported by NSFC grants 41674073 and the Project of National Deep Exploration Technology and Experimental Research (Grant number: SinoProbe-09-02(201011079)). G.A.P. acknowledges funding from a NERC Independent Research Fellowship (NE/P017266/1).

Availability of data and materials

Not applicable.

Ethics approval and consent to participate

Not applicable.

Consent for publication

Not applicable.

Competing interests

Not applicable.

Author details

[1] State Key Laboratory of Lithospheric Evolution, Institute of Geology and Geophysics, Chinese Academy of Sciences, Beijing 100029, China. [2] Research School of Earth Sciences, Australian National University, Canberra, ACT 2601, Australia. [3]Key Laboratory of Earth and Planetary Physics, Institute of Geology and Geophysics, Chinese Academy of Sciences, Beijing 100029, China. [4] Department of Earth, Ocean and Ecological Sciences, University of Liverpool, Liverpool L69 7ZE, UK. [5] Key Laboratory of Submarine Geosciences and Prospecting Techniques, Ministry of Education, and College of Marine Geosciences, Ocean University of China, 266100 Qingdao, P.R. China. [6] Department of Marine Science and Engineering, Southern University of Science and Technology, Shenzhen 518055, China.

References

Budnik K, Machczynski W (2011) Modeling magnetic field in the vicinity of a single wire helix. *Computer Applications in Electrical Engineering* 9: 69-77.

Chamalaun FH, Porath H (1968) A continuous thermal demagnetizer for rock magnetism. Pure and Applied Geophysics 70(1): 105-109.

Collinson, DW (1975) Instruments and techniques in paleomagnetism and rock magnetism. Reviews of Geophysics 13(5): 659-686.

Collinson DW (1983) *Methods in Rock Magnetism and Paleomagnetism: techniques and*

Instrumentation. London, Chapman and Hall.

Freake SM, Thorp TL (1971) Shielding of Low Magnetic Fields with Multiple Cylindrical Shells. *Review of Scientific Instruments* 42:1411. doi: 10.1063/1.1684894

Heller F, Scriba H, Weber M (1970) A Furnace for Magnetic Investigations of Rocks. Geophysical Journal International 21(5): 531-534.

Hagel R, Gong L, Unbehauer R (1994) On the magnetic field of an infinitely long helical line current, *IEEE Transactions on Magnetics* 30: 80-84. 10.1109/20.272518

Herrmannsfeldt WB, Salsburg BL (1964) Demagnetization of Magnetic Shield in the Presence of the Earth's Field, *Review of Scientific Instruments* 35:906. doi: 10.1063/1.1746861

Holm EJ, Verosub KL (1988). An analysis of the effects of thermal demagnetization on magnetic carriers. *Geophysical Research Letter* 15: 487-490.

Irving E, Robertson WA, Stott PM, Tarling D, Ward MA (1961) Treatment of partially stable sedimentary rocks showing planar distribution of directions of magnetization. *Journal of Geophysical Research* 66:1927-1933. https://doi.org/10.1029/JZ066i006p01927

Jiang ZX, Liu QS, Dekkers MJ, Zhao X, Roberts AP, Yang ZY, Jin CS, Liu JX (2017) Remagnetization mechanisms in Triassic red beds from South China. *Earth and Planetary Science Letters* 479:219-230. doi: 10.1016/j.epsl.2017.09.019

Li S, Yang Z, Deng CL, He HY, Qin HF, Sun L (2017) Clockwise rotations recorded in redbeds from the Jinggu Basin of northwestern Indochina. *Geological Society of America Bulletin* 129:1100-1122. doi: 10.1130/b31637.1

Ozaki M, Suzuki H, Takahashi K, Matijevic E (1986). Reversible ordered agglomeration of hematite particles due to weak magnetic-interactions. *Journal of Colloid and Interface Science* 113(1): 76-80.

Paterson GA, Biggin AJ, Yamamoto Y, Pan YX (2012) Towards the robust selection of Thellier-type paleointensity data: The influence of experimental noise, *Geochemistry*, *Geophysics*, *Geosystems* 13:Q05Z43. doi: 10.1029/2012GC004046

Schmidt PW (1993) Paleomagnetic cleaning strategies. *Physics of the Earth and Planetary Interiors* 76:169–178. https://doi.org/10.1016/0031-9201(93)90066-I

Sugimoto T, Sakata K, Muramatsu A (1993). Formation Mechanism of Monodisperse Pseudocubic [alpha]-Fe2O3 Particles from Condensed Ferric Hydroxide Gel. *Journal of Colloid and Interface Science*, 159(2): 372-382.

Shaw J (2010) Comment on "A new high-precision furnace for paleomagnetic and paleointensity studies: Minimizing magnetic noise generated by heater currents inside traditional thermal demagnetizers" by Zhong Zheng, Xixi Zhao, and Chorng-Shern Horng, *Geochemistry Geophysics Geosystems* 11:Q11Y11. doi: 10.1029/2010GC003211

Stephenson A (1983) Changes in direction of the remanence of rocks produced by stationary alternating field demagnetization, *Geophysical Journal Royal Astronomical Society* 73:213-239. DOI: 10.1111/j.1365-246X.1983.tb03815.x

Tarduno JA, Cottrell RD, Davis WJ, Nimmo F, Bono RK (2015) A Hadean to Paleoarchean geodynamo recorded by single zircon crystals. Science 349(6247): 521-524

Thellier E (1966) Methods and apparatus for alternating current and thermal demagnetization in *Methods and Techniques in Geophysics*, vol. 2, edited by S. K. Runcorn, pp. 205-249, Interscience, London.

Thiel F, Schnabel A, Knappe-Grüneberg S, Stollfuß D, Burghoff M (2007) Demagnetization of magnetically shielded rooms. *Review of Scientific Instruments* 78:035106. doi: 10.1063/1.2713433

Wang H, Weiss BP, Bai XN, Downey BG, Wang J, Wang J, Suavet C, Fu FF, Zucolotto ME (2017) Lifetime of the solar nebula constrained by meteorite paleomagnetism. Science 355: 623-627

Wasilewski PJ (1969) Thermochemical Remanent Magnetization (TCRM) in Basaltic Rocks. Journal of geomagnetism and geoelectricity 21(3): 595-613.

Weiss BP, Gattacceca J, Stanley S, Rochettte P, Christensen UR (2010) Paleomagnetic record of meteorites and early planetesimal Differentiation. *Space Science Reviews* 152:341-390. doi: 10.1007/s11214-009-9580-z

Yan Y, Huang B, Zhang D, Charusiri P, Veeravinantanakul A (2018) Paleomagnetic study on the Permian rocks of the Indochina Block and its implications for paleogeographic configuration and northward drifting of Cathaysialand in the Paleo-Tethys. *Journal of Geophysical Research: Solid Earth* 123: 4523–4538. doi: 10.1029/2018JB015511

Yang T, Jin J, Bian W, Ma Y, Gao F, Peng W, Ding J, Wang S, Zhang S, Wu H, Li H, Yang Z (2019) Precollisional Latitude of the Northern Tethyan Himalaya From the Paleocene Redbeds and Its Implication for Greater India and the India-Asia collision. *Journal of*

Geophysical Research: Solid Earth 124: 10777-10798.

Yuan J, Yang ZY, Deng CL, Krijgsman W, Hu XM, Li SH, Shen ZS, Qin HF, An W, He HY, Ding L, Guo ZT, Zhu RX (2020) Rapid drift of the Tethyan Himalaya terrane before two-stage India-Asia collision. National Science Review doi: 10.1093/nsr/nwaa173

Zheng Z, Zhao X, Horng CS (2010a) A new high precision furnace for paleomagnetic and paleointensity studies: Minimizing magnetic noise generated by heater currents inside traditional thermal demagnetizers. *Geochemistry Geophysics Geosystems* 11: Q04Y08. doi: 10.1029/2010GC003100

Zheng Z, Zhao X, Horng CS (2010b) Reply to comment by John Shaw on "A new high-precision furnace for paleomagnetic and paleointensity studies: Minimizing magnetic noise generated by heater currents inside traditional thermal demagnetizers", *Geochemistry Geophysics Geosystems* 11:Q11Y12. doi:10.1029/2010GC003295

Figure 1. Configuration of non-inductive heating wires. (a) Bifilar solenoid wrapped for a small oven, (b) solenoid-like helical heating wires arranged in a larger oven, (c) the new straight core solenoid heating wires using in the TD-PGL-100. Arrows indicate the current flow direction.

Figure 2. Schematic diagram for calculating magnetic field outside of solenoid (R is the radius of solenoid, $p = 2\pi a$ is the pitch distance and d is the distance between point P and central axis of solenoid).

Figure 3. Magnetic field simulations of single long solenoid at (a) 10 mm and (b) 20 mm from the central axis. The black symbol represents the result of conventional solenoid and the red symbol represents the result of a solenoid with a reverse straight wire at solenoid axis. Insets in (b) show detail measurements over the central 50 cm highligthing period nature of the field, which is caused by the solenoid pitch.

Figure 4. Contour map of magnetic field distribution on different components in middle cross section of the furnace with composed of 12 conventional solenoids (a,b,c) and new heating elements (d,e). (f)The position of the solenoids and the corresponding current direction in adjacent. Letter X, Y, Z in the middle of the graph represents the direction of the magnetic field.

Figure 5. Contour map of magnetic field distribution if the solenoids are wired such that the current flow is parallel. (a, b, c) the field distribution with composed of 12 conventional solenoids, and (d,e) the field distribution with new heating elements. (f) The position of the solenoids and the corresponding current direction in adjacent. Letter X, Y, Z in the middle of the graph represents the direction of the magnetic field.

Figure 6. Magnetic field measurement of conventional solenoid (a) and new heating wire (b). (c) Current field at different positions, the black line represents the result of conventional solenoid and the red dash line represents the result of a straight core solenoid. The length of solenoid is 1

meter, the radius is 4 mm and with pitch distance of 4 mm. The DC current of 1 A applied in the wire during measurement.

Figure 7. (a) Photo of the new furnace chamber. (b) Current field (red triangles) with 1A applied to the heating wire along longitude axis in the newly designed furnace (Multiple curves represent different vertical distances from the central axis). (c) Current field with 1A applied to the heating wire along longitude axis in conventional furnace, the current of adjacent solenoids is opposite. (d) Current field with 1A applied to the heating wire along longitude axis in conventional furnace, currents of adjacent solenoids in each group are opposite, but two groups in parallel connect.

Figure 8. (a) Toroidal degaussing coil embodying the shield cylinder. (b) Residual fields (black circles) along longitude axis in the newly designed furnace

Figure 9. Temperature curves during heating and cooling at different target temperatures in a thermal demagnetization experiment

Figure 10. Thermal decay curves and corresponding orthogonal plots of progressive thermal demagnetization of natural specimens. Solid (open) circles indicate projection on the horizontal (vertical) plane.

Figures

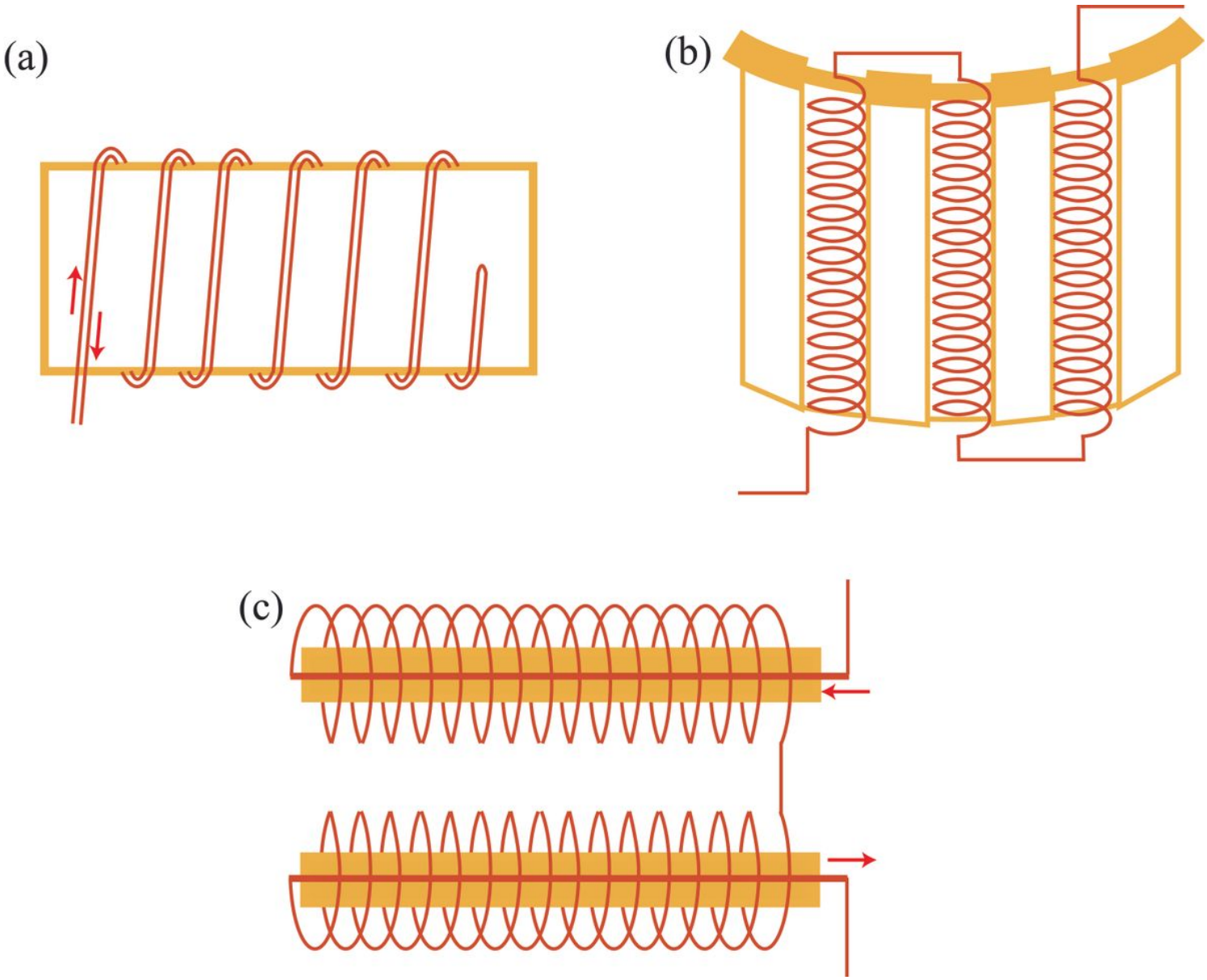

Figure 1

Configuration of non-inductive heating wires. (a) Bifilar solenoid wrapped for a small oven, (b) solenoid-like helical heating wires arranged in a larger oven, (c) the new straight core solenoid heating wires using in the TD-PGL-100. Arrows indicate the current flow direction.

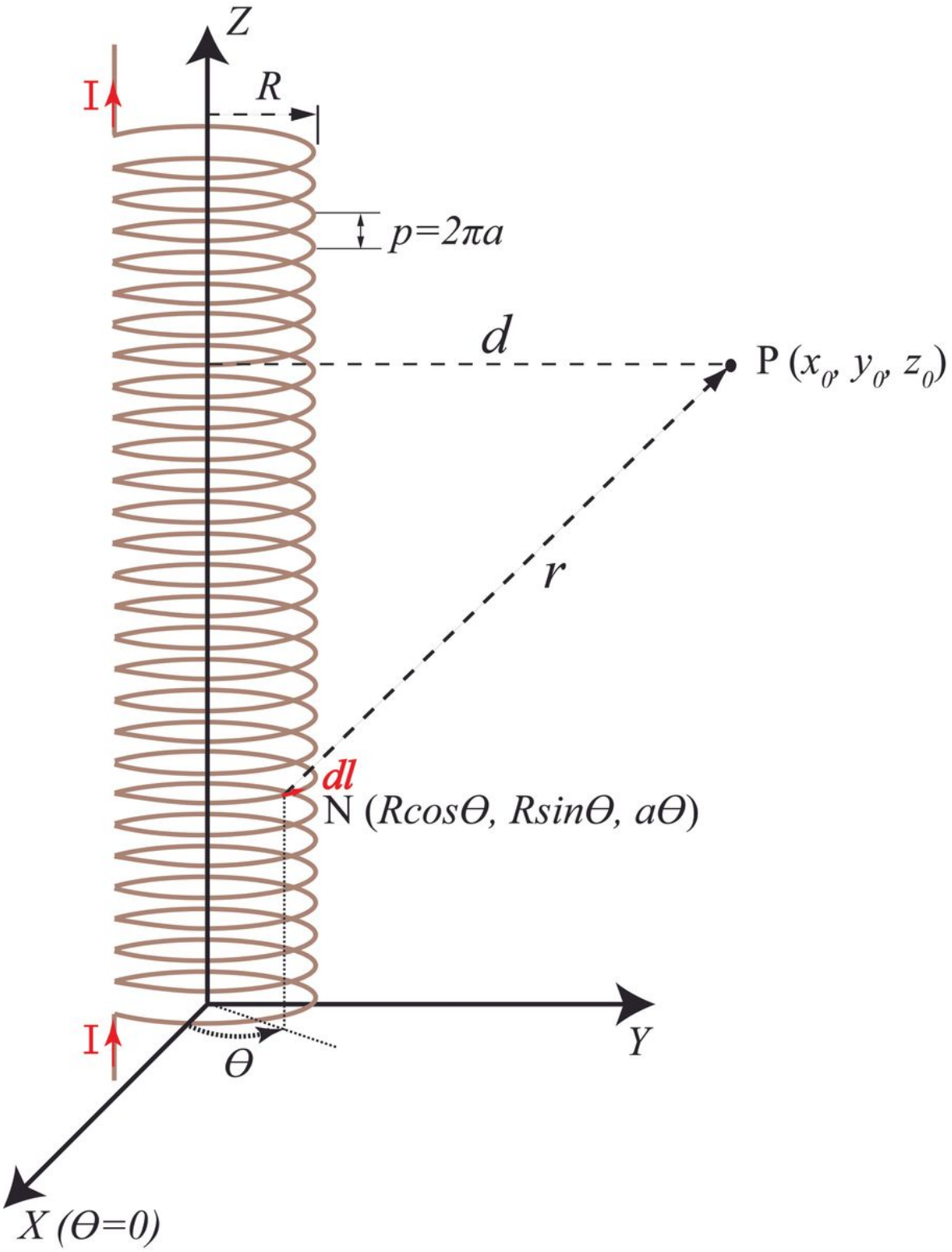

Figure 2

Schematic diagram for calculating magnetic field outside of solenoid (R is the radius of solenoid, p = 2πa is the pitch distance and d is the distance between point P and central axis of solenoid).

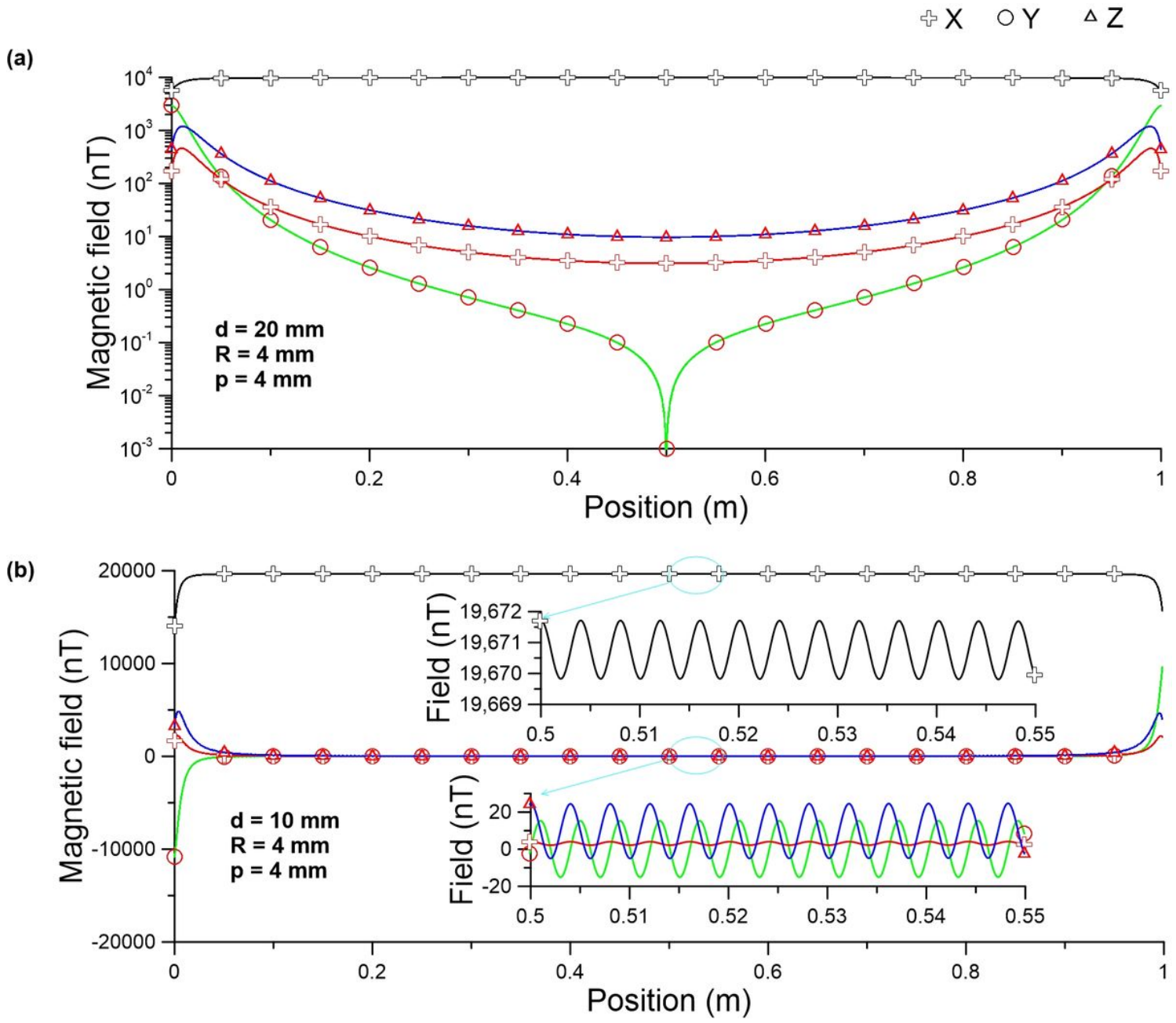

Figure 3

Magnetic field simulations of single long solenoid. The black symbol represents the result of conventional solenoid and the red symbol represents the result of a solenoid with a reverse straight wire at solenoid axis.

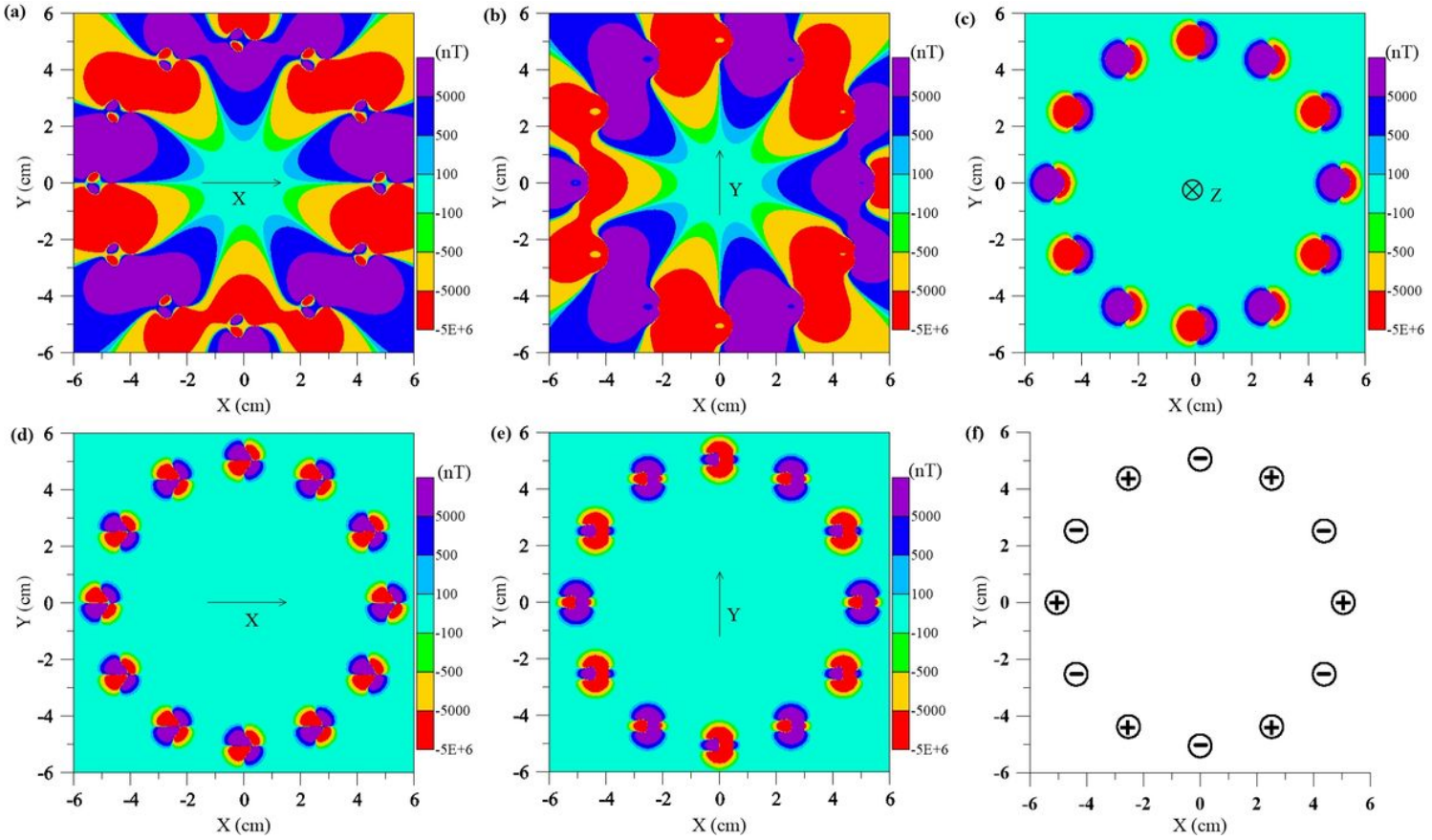

Figure 4

Contour map of magnetic field distribution on different components in middle cross section of the furnace with composed of 12 conventional solenoids (a,b,c) and new heating elements (d,e). (f)The position of the solenoids and the corresponding current direction in adjacent. Letter X, Y, Z in the middle of the graph represents the direction of the magnetic field.

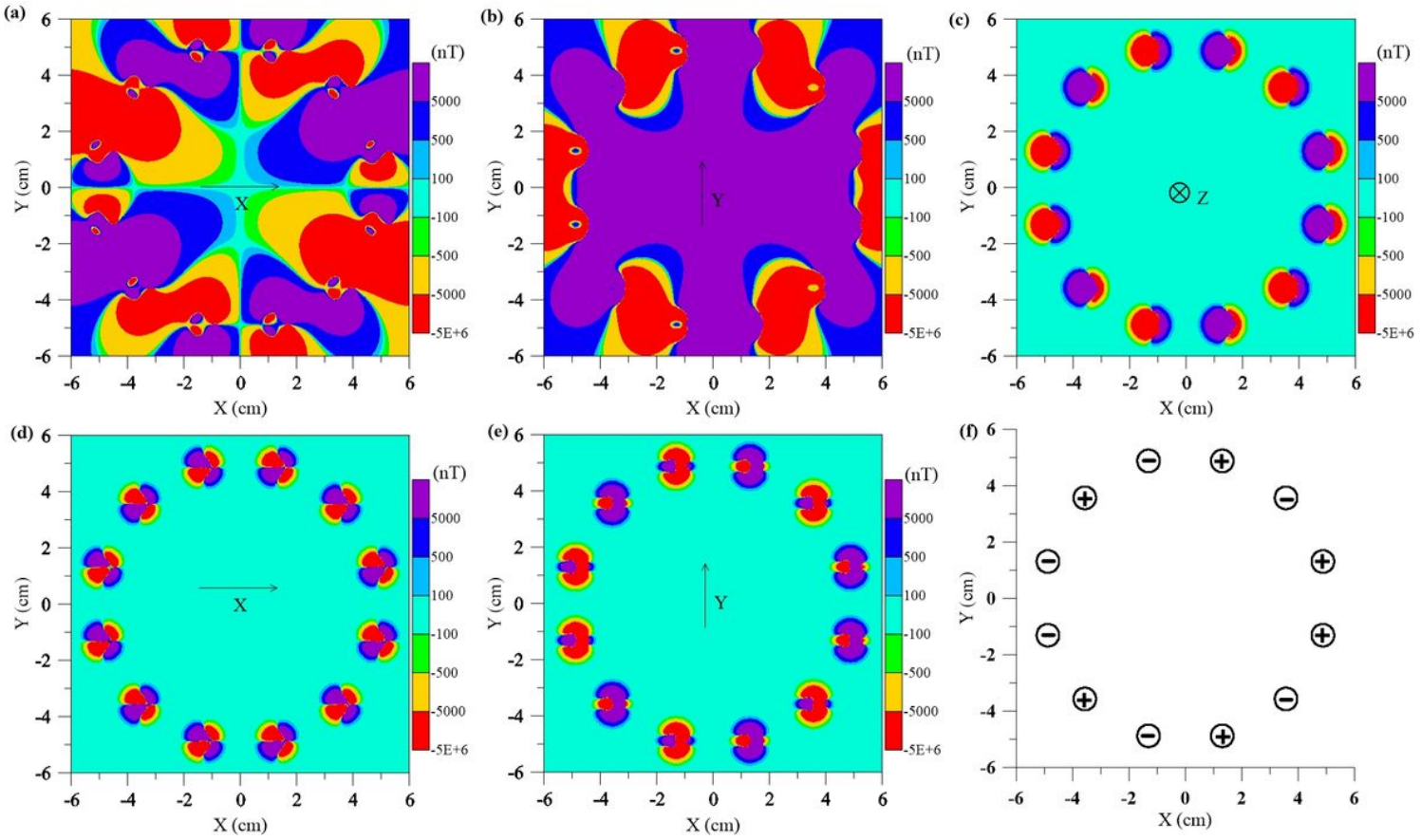

Figure 5

Contour map of magnetic field distribution on different components with different way of wire connection from Figure 4. (a, b, c) the field distribution with composed of 12 conventional solenoids, and (d,e) the field distribution with new heating elements. (f) The position of the solenoids and the corresponding current direction in adjacent. Letter X, Y, Z in the middle of the graph represents the direction of the magnetic field.

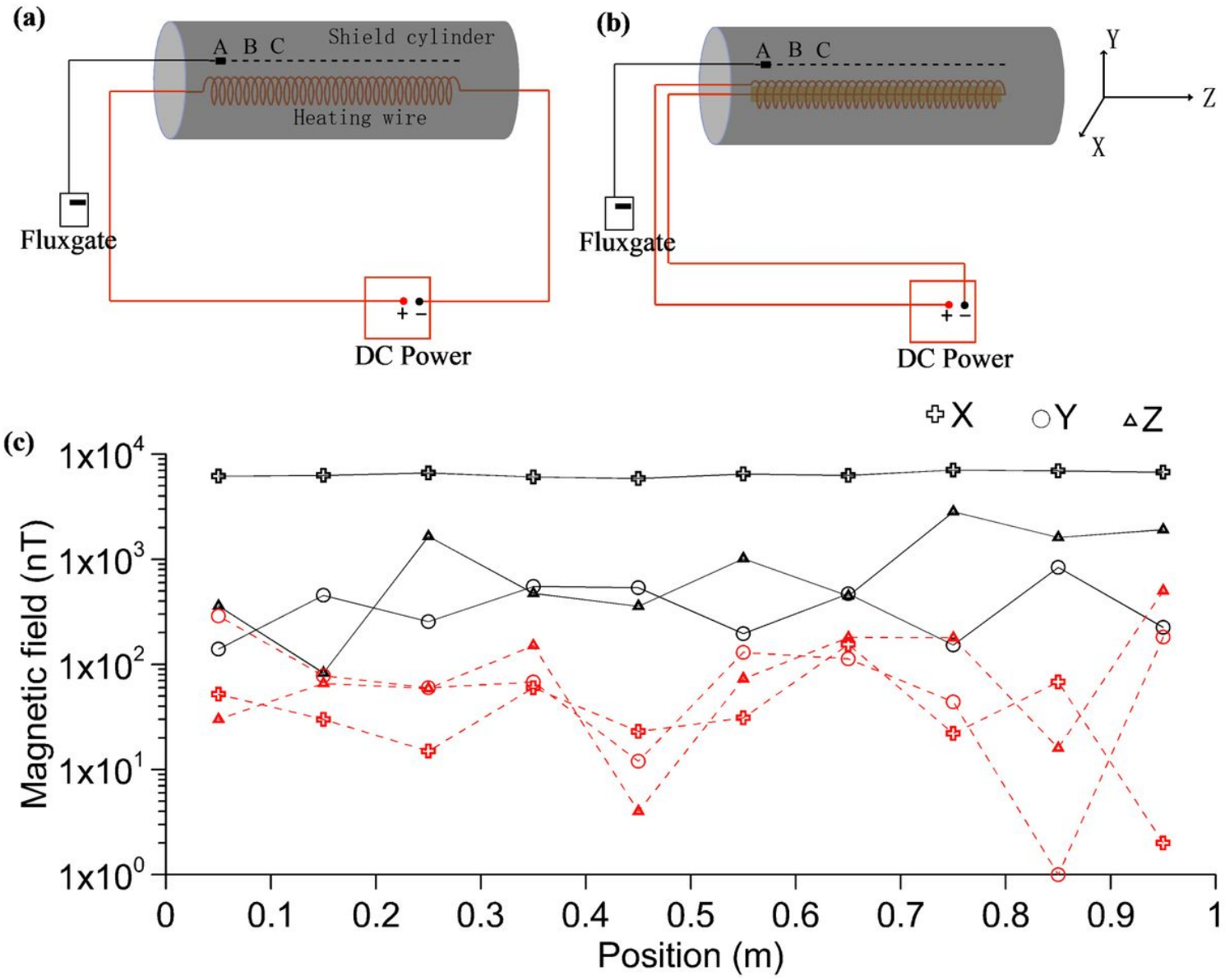

Figure 6

Magnetic field measurement of conventional solenoid and new heating wire. The length of solenoid is 1 meter, the radius is 4 mm and with pitch distance of 4 mm. The DC current of 1 A applied in the wire during measurement. The black line represents the result of conventional solenoid and the red dash line represents the result of a straight core solenoid.

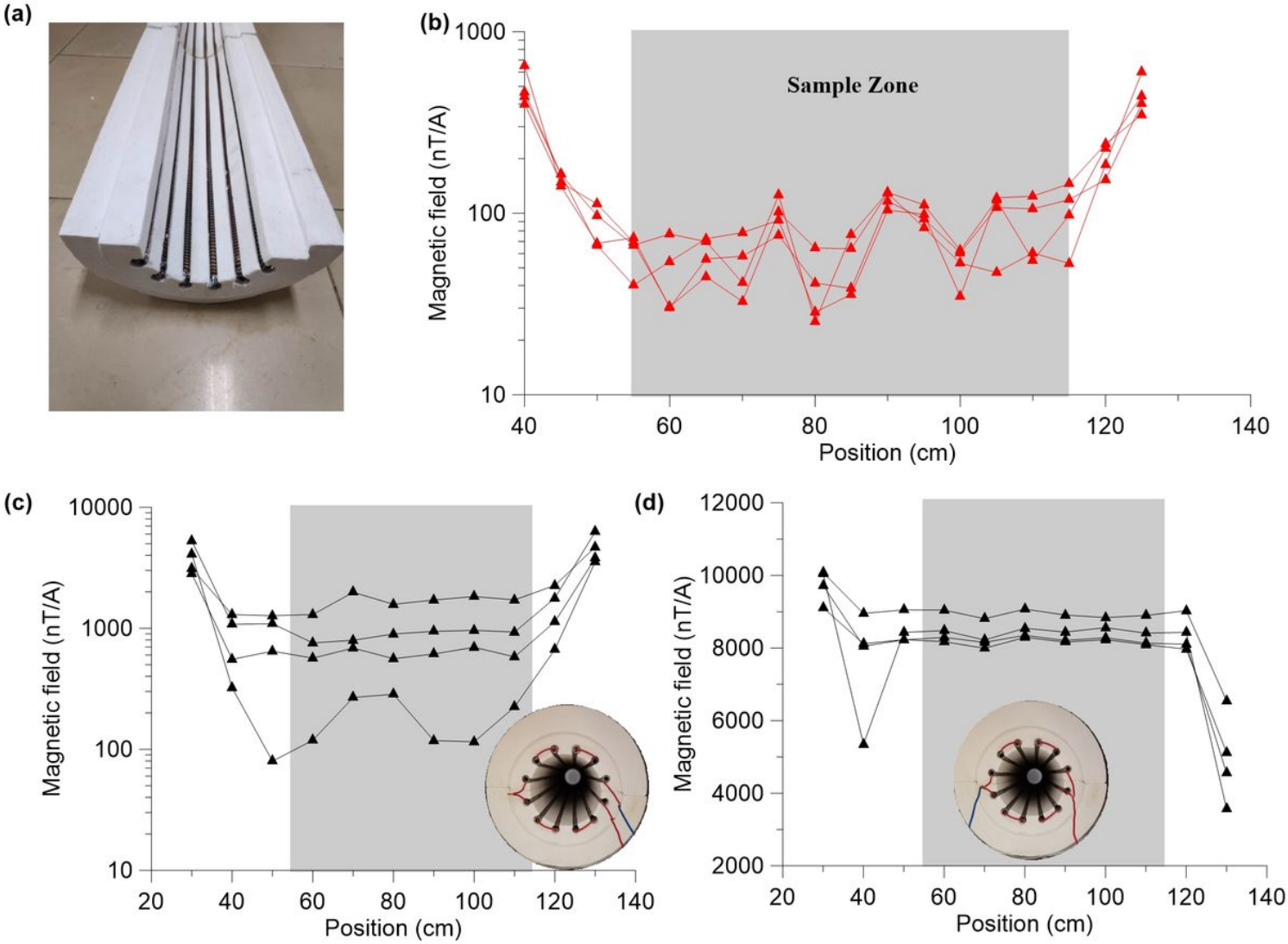

Figure 7

(a) Photo of furnace chamber. (b) Current field (red triangles) with 1A applied to the heating wire along longitude axis in the newly designed furnace (Multiple curves represent different vertical distances from the central axis). (c) Current field with 1A applied to the heating wire along longitude axis in conventional furnace, the current of adjacent solenoids is opposite. (d) Current field with 1A applied to the heating wire along longitude axis in conventional furnace, currents of adjacent solenoids in each group are opposite, but two groups in parallel connect.

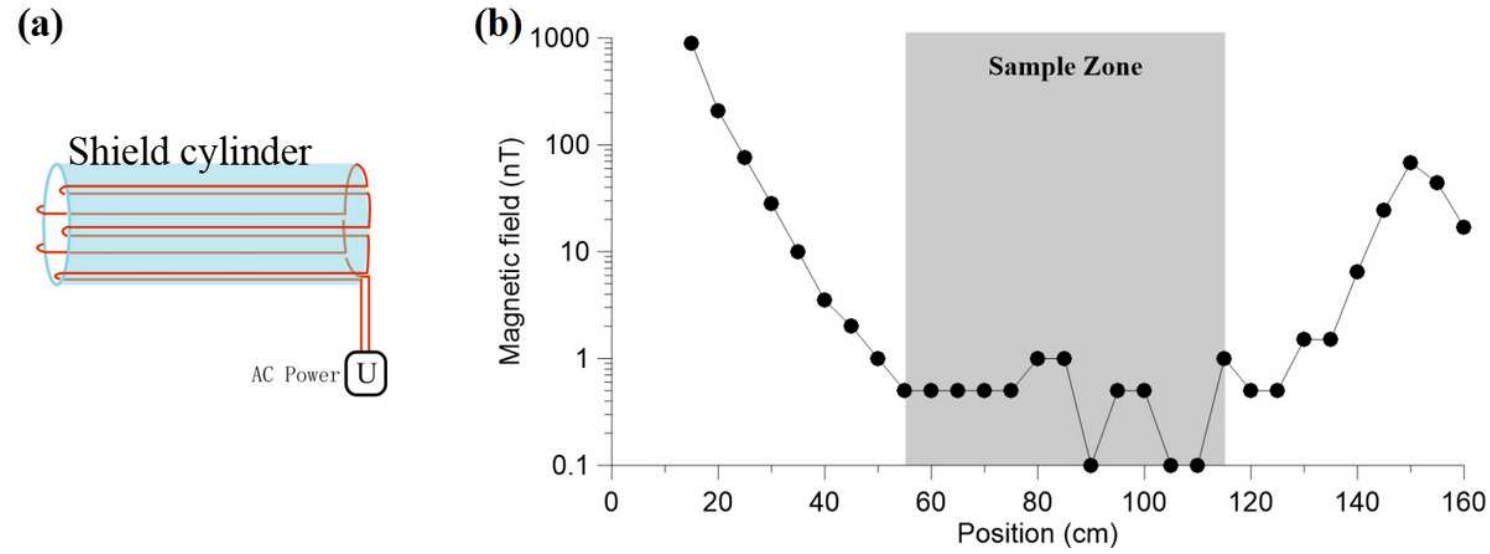

Figure 8

(a) Toroidal degaussing coil embody the shield cylinder. (b) Residual fields (black circles) along longitude axis in the newly designed furnace

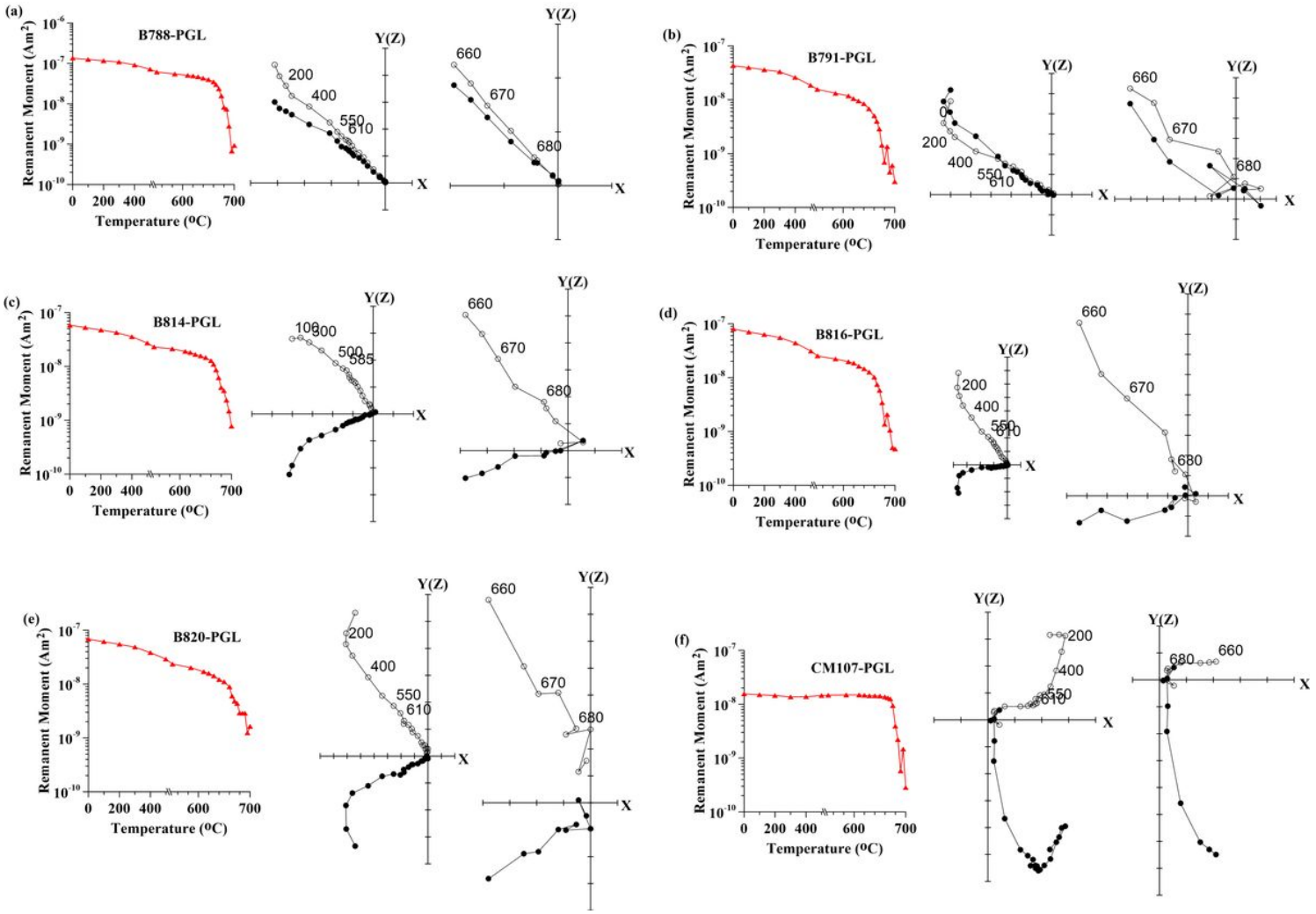

Figure 9

Thermal decay curves and corresponding orthogonal plots of progressive thermal demagnetization of natural specimens. Solid (open) circles indicate projection on the horizontal (vertical) plane.

Supplementary Files

This is a list of supplementary files associated with this preprint. Click to download.

- FigureS1.jpg
- FigureS2.jpg
- supplement3.docx